LBL-17739
Preprint c.2

Lawrence Berkeley Laboratory

UNIVERSITY OF CALIFORNIA

RECEIVED
LAWRENCE
BERKELEY LABORATORY

DEC 11 1985

LIBRARY AND
DOCUMENTS SECTION

Materials & Molecular Research Division

To be submitted to the Journal of the
Electrochemical Society

A MATHEMATICAL MODEL FOR THE PERIODIC ELECTRODEPOSITION OF MULTICOMPONENT ALLOYS

M.W. Verbrugge and C.W. Tobias

August 1984

TWO-WEEK LOAN COPY

This is a Library Circulating Copy
which may be borrowed for two weeks.

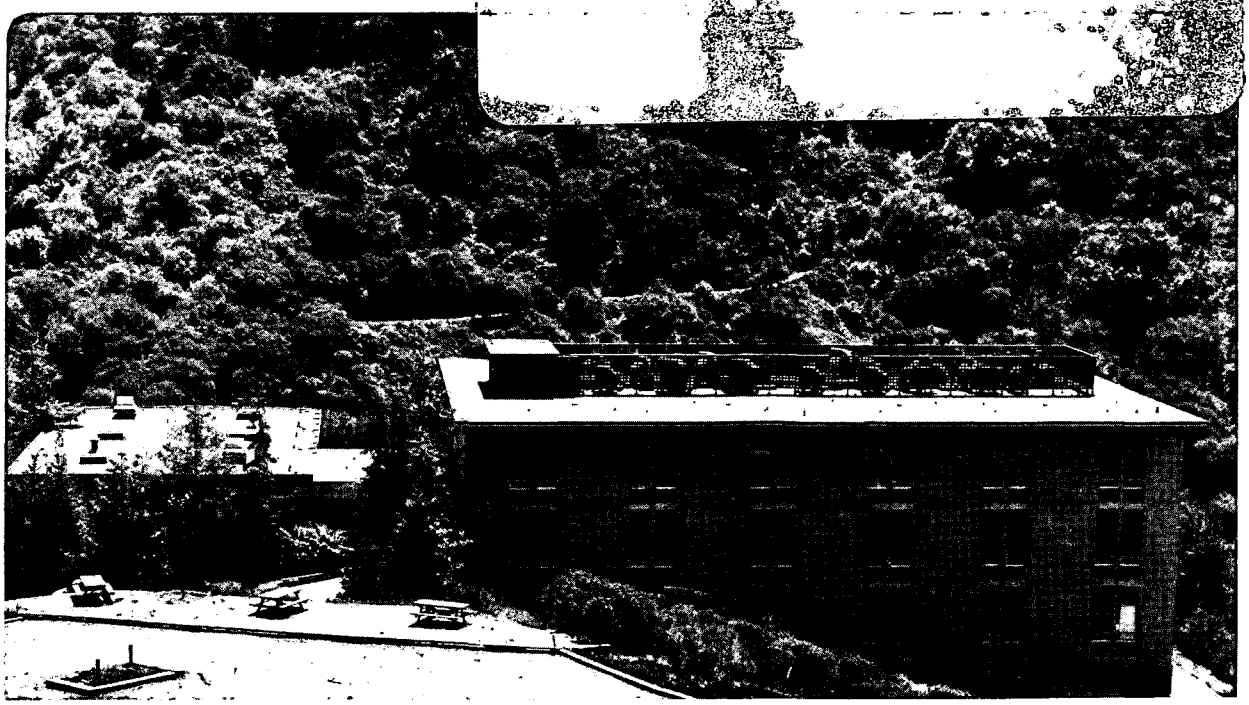

LBL-17739 c.2

Prepared for the U.S. Department of Energy under Contract DE-AC03-76SF00098

DISCLAIMER

This document was prepared as an account of work sponsored by the United States Government. While this document is believed to contain correct information, neither the United States Government nor any agency thereof, nor the Regents of the University of California, nor any of their employees, makes any warranty, express or implied, or assumes any legal responsibility for the accuracy, completeness, or usefulness of any information, apparatus, product, or process disclosed, or represents that its use would not infringe privately owned rights. Reference herein to any specific commercial product, process, or service by its trade name, trademark, manufacturer, or otherwise, does not necessarily constitute or imply its endorsement, recommendation, or favoring by the United States Government or any agency thereof, or the Regents of the University of California. The views and opinions of authors expressed herein do not necessarily state or reflect those of the United States Government or any agency thereof or the Regents of the University of California.

LBL-17739

A MATHEMATICAL MODEL FOR THE PERIODIC ELECTRODEPOSITION OF MULTICOMPONENT ALLOYS

by

Mark W. Verbrugge and Charles W. Tobias

Lawrence Berkeley Laboratory
University of California
Berkeley, California 94720

This work was supported by the Director,
Office of Energy Research, Office of Basic Energy Sciences,
Materials Sciences Division of the Office of the
U.S. Department of Energy, under Contract No. DE-AC03-76SF00098

A MATHEMATICAL MODEL FOR THE PERIODIC ELECTRODEPOSITION OF MULTICOMPONENT ALLOYS

Mark W. Verbrugge and Charles W. Tobias

Lawrence Berkeley Laboratory
University of California
Berkeley, California 94720

Abstract

A mathematical model is presented for the electrodeposition of multicomponent alloys by an arbitrarily specified current source. The model takes into consideration transient convective mass transfer to a rotating disk electrode, Butler-Volmer kinetics, and individual component activities in the electrodeposit. The model can be used to calculate current-potential relationships, ionic concentration profiles, and electrodeposit composition. Results for square-pulse, pulse-reversal, and triangular current waveforms are presented. An analogous model for potential-controlled electrolysis is also discussed.

Introduction

The properties of alloys vary over a wider range than those of their parent metals, and thus can often be designed to better fulfill the mechanical and chemical requirements of our civilization. Electrodeposition offers several unique advantages for the formation of alloys. The superior control of the alloy composition, including the formation of non-equilibrium alloys, and the ability to prepare thin films are well documented. Brenner's encyclopedic monograph (1) reviews some practical methods for the electrodeposition of various alloys and Gorbunova and Polukarov's treatment (2) outlines the fundamental principles involved.

It has long been known that pulsing the current can profoundly affect the nature of single-component electrodeposits. Although the pulsed plating of alloys has received comparatively little attention, it has been observed that the phase structure and morphology of alloy deposits can be altered by changing the characteristics of the pulsed-current waveform. This work presents a model for predicting the current-potential relationship and the composition profiles in the electrodeposit and the electrolyte.

Wan et al. (3) have presented a literature review dealing with the application of pulsed-plating techniques for single-component metal deposition. Avila and Brown (4) have cited the following advantages of pulsed plating over dc electroplating: 1) extremely dense and highly conductive deposits, 2) a reduced need for plating additives, and 3) increased plating rates. In reference to the last advantage, Cheh (5) has shown analytically that pulsed-current plating can never attain a higher average plating rate than dc plating at the diffusion-limited current. However, a higher average current density is often used in pulse plating, relative to dc plating, since poor quality electrodeposits are often formed under dc conditions near the diffusion-limiting current. Lamb (6) has investigated the mechanical properties of single-component copper and silver electrodeposits obtained by current pulses in the microsecond range. Puippe and Ibl (7)

studied the morphology of pulse-plated cadmium, copper, and gold electrodeposits. The influence of the off-time, the pulse-current density, and the length of the pulse time were analyzed. Different morphological trends were observed and discussed for the different chemical systems. Despic and Popov (8) examined the effect of a pulsating potential on the morphology of copper and zinc electrodeposits. Typical results illustrated that increasing the frequency led to a progressively smoother deposit. Popov (9) also has reviewed some approaches to the quantitative modeling of the surface-roughness amplification during an electrodeposition process. Sullivan (10) has reported that high-current-density pulse-plating of cobalt results in significantly stronger and harder electrodeposits.

The pulsed plating of multicomponent electrodeposits has received less attention than pure-component electrodeposition. Gelchinski et al. (11) electroplated chromium-cobalt alloys using a pulsed-potential source. Mirror bright electrodeposits containing supersaturated solid solutions were obtained. It has been observed that the structure and the physical properties of the electrodeposited alloys can be very different from the thermally prepared alloys of similar composition. Gelchinski et al. also found that a change in the electrodeposition conditions can cause a marked change in the phase structure of the electrodeposit, even for those deposits of identical chemical composition. Burrus (12) has described various conditions where the pulsed plating of different metals and metal mixtures can be used advantageously. Leidheiser and Ghuman (13) used a pulsed-current setup to electrodeposit silver-tin alloys which could be easily polished to a high luster. Cohen et al. (14) have electroplated cyclic, multilayered, alloy-coatings of varying silver and palladium composition with square-pulse and triangular current waveforms. They also report on periodic-potential plating studies of various multicomponent electrodeposits.

Mathematical Analysis

In considering the mathematical modeling for the electrodeposition of multicomponent alloys, it is convenient to divide the problem into three interrelated

parts: the liquid phase containing the discharging ions, the electrolyte-electrodeposit interface, and the electrodeposited alloy.

The Liquid Phase

One of the goals of this work is to quantitatively predict the ionic surface-concentrations throughout the electrodeposition process. It has been well established that the ionic surface concentrations can greatly influence the electrodeposit composition and morphology (15,16).

A theoretical analysis for single-component mass transfer in pulsed electrolysis was recently published by Chin (17). A stagnant (Nernst) diffusion layer was assumed valid in order to develop a comprehensive theory for pulsed electrolysis. Chin's paper includes a brief review of previous theoretical studies in single-component pulsed electrolysis.

Since our treatment uses a current-step solution and the method of superposition to derive a model for multicomponent mass transfer, we shall review some current-step solutions which can be used with this technique. The method of superposition is computationally very efficient, although the differential equations describing the process must be linear for this method to be applied. Thus migration effects are not included in this model. Double layer charging is also not considered. Since practical plating baths usually contain an excess of supporting electrolyte, migration effects can often be neglected. Double layer charging effects can become important in an electrodeposition process if microsecond current cycles are used (18). Before proceeding, it should be mentioned that attempts have been made to qualitatively describe multicomponent, pulsed-current processes (19–22). Also, Cheng and Cheh have presented finite-difference models for the pulsed-current electrodeposition of copper with hydrogen evolution (23) and of lead-tin alloys (24).

The convective diffusion equation for the one-dimensional mass transport of species i is

$$\frac{\partial c_i}{\partial t} + v_y \frac{\partial c_i}{\partial y} = D_i \frac{\partial^2 c_i}{\partial y^2} \quad . \qquad [1]$$

For high Schmidt numbers, the appropriate expression for the normal component of the fluid velocity to a rotating disk electrode (RDE) is (25,26)

$$v_y = -0.51023\, \omega^{3/2} \nu^{-1/2} y^2 \quad . \qquad [2]$$

The radial variation of the ionic surface concentration is neglected in this treatment, as it would considerably complicate the problem (27–29). For small disks this is a good approximation.

For the current-step problem, the initial condition and boundary conditions are

$$c_i(0,y) = c_i^b \qquad [3]$$

$$c_i(t,\infty) = c_i^b \qquad [4]$$

$$\frac{\partial c_i(t,0)}{\partial y} = \frac{-i(0)}{n_i F D_i} \quad , \qquad [5]$$

where the electrode reaction for metal deposition is

$$M_i^{n_i+} + n_i e^- \underset{k_{a,i}}{\overset{k_{c,i}}{\rightleftharpoons}} M_i \quad . \qquad [6]$$

Krylov and Babak (30) have obtained an analytic series solution for the current-step problem stated by Eqs. [1]–[5]. However, the solution does not converge for long times (31). Niscancioglu and Newman (32) numerically calculated an alternate series solution which is valid for long times and can be used in conjunction with a short-time, asympototic series representation of Krylov and Babak's solution.

Niscancioglu and Newman's long-time solution is

$$c_i = c_i^b + \frac{i_i\delta_i}{n_iFD_i\Gamma(4/3)}\left\{\int_{\frac{\Gamma(4/3)y}{\delta_i}}^{\infty} e^{-x^3}dx - \sum_{k=1}^{\infty} B_kZ_k\left[\frac{y\Gamma(4/3)}{\delta_i}\right]e^{-\lambda_kD_it\left[\frac{\Gamma(4/3)}{\delta_i}\right]^2}\right\} . \qquad [7]$$

The values of B_k, Z_k, and λ_k are given in Refs. (18) and (32).

The first few terms of the short-time, asymptotic series representation of Krylov and Babak's solution is

$$c_i = c_i^b + \frac{2i_i\sqrt{t}}{n_iF\sqrt{\pi D_i}}\left\{1 - \frac{\sqrt{\pi}}{16}\left[\frac{D_it}{\left(\frac{\delta_i}{3^{1/3}\Gamma(4/3)}\right)^2}\right]^{3/2} + \frac{1}{420}\left[\frac{D_it}{\left(\frac{\delta_i}{3^{1/3}\Gamma(4/3)}\right)^2}\right]^3 + \cdots\right\} \qquad [8]$$

In Eqs. [7] and [8], δ_i is the Levich diffusion layer thickness (33)

$$\delta_i = 1.612\left(\frac{D_i}{\nu}\right)^{1/3}\left(\frac{\nu}{\omega}\right)^{1/2} , \qquad [9]$$

which is the characteristic distance for long times.

More approximate representations for the current-step problem have also yielded relatively accurate results. In a classic treatment, Roseburgh and Lash Miller (34) derived an analytic solution for the current-step problem by replacing Eq. [1] with the equation representing Fick's second law of diffusion and Eq. [4] by

$$c_i(t,\delta_i) = c_i^b \quad . \qquad [10]$$

This solution is presented in the Appendix.

Roseburgh and Lash Miller used the method of superposition on their current-step solution to describe single-component mass transfer with a periodic current source (34). Cheh et al. (5,35,36) have made use of this solution by comparing it with some experimental results. Visawanathan and Cheh (37) and Hale (38) have presented numerical solutions to Eqs. [1]–[5] and compared their solutions to that of Roseburgh and Lash Miller. (Hale actually compared his

solution to Siver's solution (39), which Siver had in turn referenced to Roseburgh and Lash Miller.) The error was always less than 4 percent. Visawanathan et al. (40) numerically solved the system of Eqs. [1] through [4], with a pulsed-current boundary condition in place of Eq. [5], and compared this to Roseburgh and Lash Miller's analytic solution for a pulsed-current source. The agreement between the two solutions was excellent.

Thus far, we have reviewed one analytical current step solution (that assumes a Nernst diffusion layer) and three numerical solutions. For the problem we address in this paper, we require a current-step solution for short and long times. There is very little extra numerical effort involved in using Eqs. [7] instead of Eq. [A–2], especially if only the surface concentrations of the discharging ions are required. For this reason, we have chosen to use Eqs. [7] and [8], along with the method of superposition, to model the ionic mass transfer. This restricts our treatment to a RDE. The procedure to be used for other systems which can be modeled accurately with a Nernst diffusion layer is presented in the Appendix. A comparison between the two methods is shown in Fig 2.

Using the method of superposition on Equation [7], the concentration expression for an arbitrarily-specified current source is

$$c_i = i_{i,n}\,\Theta_{i,n} + \Psi_{i,n}\ , \qquad [11]$$

where

$$\Theta_{i,n} = \frac{\delta_i}{n_i F D_i \Gamma(4/3)} \left\{ \int_{\frac{y\Gamma(4/3)}{\delta_i}}^{\infty} e^{-x^3} dx - \sum_{k=1}^{\infty} B_k Z_k e^{-\lambda_k D_i \left[\frac{\Gamma(4/3)}{\delta_i}\right]^2 (t-t_{n-1})} \right\} \qquad [12]$$

and

$$\Psi_{i,n} = c_i^b +$$

$$\frac{\delta_i}{n_i F D_i \Gamma(4/3)} \left\{ \sum_{j=1}^{\infty} i_{i,j} \sum_{k=1}^{\infty} B_k Z_k \left[e^{-\lambda_k D_i \left[\frac{\Gamma(4/3)}{\delta_i}\right]^2 (t-t_{j-1})} - e^{-\lambda_k D_i \left[\frac{\Gamma(4/3)}{\delta_i}\right]^2 (t-t_j)} \right] \right\} . \quad [13]$$

The current source has been expressed as n discrete current steps. The method of superposition has been used previously for single-component, pulsed-current chronopotentiometry by Andricacos and Cheh (41), and there are a number of references in the literature which can be consulted to derive Eqs. [11], [12], and [13] (34,42,43).

For short times, the series in Eqs. [12] and [13] will not converge. Equation [8] can then be used to express $\Theta_{i,n}$ and $\Psi_{i,n}$. For very short times, only the first term in Eq. [8] need be retained. Equation [8] then becomes the familiar Sand equation and δ_i drops out of the problem since there is no characteristic length for the semi-infinite linear diffusion problem. Equations [12] and [13] are then replaced by

$$\Theta_{i,n} = \frac{2\sqrt{t - t_{n-1}}}{n_i F \sqrt{\pi D_i}} \quad [14]$$

and

$$\Psi_{i,n} = c_i^b + \frac{2}{n_i F \sqrt{\pi D_i}} \sum_{j=1}^{n} i_j \left[\sqrt{t - t_{j-1}} - \sqrt{t - t_j} \right] . \quad [15]$$

Equations [14] and [15] can also be used to solve the analogous problem of multicomponent mass transfer to a stationary electrode.

The Liquid-Electrodeposit Interface

While a relatively accurate liquid-phase transport model can be developed, such an exacting and general approach is not as easily accomplished for the interface. In multicomponent electrolysis, the potential distribution across the double layer will be affected by the various discharging ions. However, in well

supported solutions, the discharging ions will not significantly influence the double-layer structure. The crystallization kinetics can also be changed, although this will not be considered in this paper. An excellent treatment of this problem can be found in the work of Fleischmann and Thirsk (44).

For the electrode reaction of component i, given by Eq. [6], a Bulter-Volmer expression will be used to describe the electrode kinetics. Specific adsorption and chemisorption are not taken into account. Thus (45)

$$\frac{i_{i,n}}{n_i F} = k_{a,i} a_{i,n} e^{(1-\beta_i) n_i f E_n} - k_{c,i} \frac{c^s_{i,n}}{\rho_o} e^{-\beta_i n_i f E_n} \quad , \qquad [16]$$

where

$$E_n = V_n + \left[U^{\theta}_{re} - \frac{1}{n_{re} f} \sum_i s_{i,re} \ln \frac{c_{i,re}}{\rho_o} \right] - i_n r \quad . \qquad [17]$$

The bracketed term in Eq [17] represents the open-circuit potential difference between the reference electrode and a standard hydrogen electrode. The potential difference between the cathode and the reference electrode is V_n. The last term in Eq. [17] accounts for the ohmic drop between the reference electrode and the cathode.

The individual currents can be obtained by substituting for $c^s_{i,n}$ in Eq. [16] using Eq. [11], evaluated at the surface, and solving for $i_{i,n}$:

$$i_{i,n} = \frac{k_{a,i} a_{i,n} e^{(1-\beta_i) n_i f E_n} - \frac{1}{\rho_o} k_{c,i} \Psi^s_{i,n} e^{-\beta_i n_i f E_n}}{\frac{1}{n_i F} + \frac{1}{\rho_o} k_{c,i} \Theta^s_{i,n} e^{-\beta_i n_i f E_n}} \qquad [18]$$

The total imposed current must equal the sum of the m individual currents:

$$\left(\sum_{i=1}^{m} i_{i,n} \right) - i_n = 0 \quad . \qquad [19]$$

Equations [18] and [19] can be combined to yield a nonlinear equation in E_n, the electrode potential. The second order Newton-Raphson algorithm (46) is used to solve the resulting equation for an arbitrary number of depositing metal

ions.

Using Eqs. [18] and [19], the function H_n is defined as

$$H_n = \left(\sum_{i=1}^{m} i_{i,n}\right) - i_n \quad . \qquad [20]$$

For the correct value of the electrode potential, H_n will be equal to zero. H_n is given by

$$H_n = \left[\sum_{i=1}^{m} \frac{k_{a,i}a_{i,n}e^{(1-\beta_i)n_i f E_n} - \frac{1}{\rho_o}k_{c,i}\Psi_{i,n}^{s}e^{-\beta_i n_i f E_n}}{\frac{1}{n_i F} + \frac{1}{\rho_o}k_{c,i}\Theta_{i,n}^{s}e^{-\beta_i n_i f E_n}}\right] - i_n \quad . \qquad [21]$$

The value of E_n is found by iteration:

$$(E_n)_{new} = (E_n)_{old} - \left[\frac{H_n}{\left(\frac{\partial H_n}{\partial E_n}\right)}\right]_{old} \quad . \qquad [22]$$

The value of the derivative in Eq. [22] is

$$\frac{\partial H_n}{\partial E_n} = \sum_{i=1}^{m} \frac{\left[\frac{k_{a,i}a_{i,n}(1-\beta_i)}{RT}e^{(1-\beta_i)n_i f E_n} + \frac{k_{c,i}\Psi_i^{s}\beta_i}{\rho_o RT}e^{-\beta_i n_i f E_n}\right]}{\left(\frac{1}{n_i F} + \frac{1}{\rho_o}k_{c,i}\Theta_i^{s}e^{-\beta_i n_i f E_n}\right)^2}$$

$$+ \frac{\left(\frac{1}{\rho_o}k_{c,i}\Theta_{i,n}^{s}k_{a,i}a_{i,n}n_i f e^{(1-2\beta_i)n_i f E_n}\right)}{\left[\frac{1}{n_i F} + \frac{1}{\rho_o}k_{c,i}\Theta_i^{s}e^{-\beta_i n_i f E_n}\right]^2} \quad . \qquad [23]$$

For each time step, the iteration scheme outlined in Eqs. [20]–[23] must be completed. However, when the previous time step's value of E_n is used to start the iteration in Eq. [22], convergence is generally obtained within 3 or 4 iterations.

It should be noted that the partial currents can be obtained explicitly in terms of E_n in Eq. [18] because the electrochemical reaction was assumed to be

first order in the concentration of the discharging metal ion concentration. This is usually the case in the electrodeposition of metals. If the reaction were not first order, it would still be relatively easy to solve numerically for the electrode potential and the partial currents.

Equation [18] is also valid for controlled-potential electrolysis. If the ohmic drop is neglected in Eq. [17], Eq. [18] yields the partial current explicitly for controlled-potential electrolysis. Since the ohmic drop can easily be subtracted out in one-dimensional systems, this does not present a major restriction.

The model we have provided for the liquid-phase mass transfer and kinetics could also be used to describe processes for the electrosynthesis of compounds by a periodic current source. Alkire and Tsai (47) have listed a number of references for the synthesis of compounds by a periodic current source.

The Electrodeposit

Two problems must be treated for a complete description of the solid-state alloy. The first problem concerns the dependence of the surface activity on the alloy composition. When experimental data are combined with the judicious choice of an activity model, the activities of the alloy components can be obtained. The second problem involves the actual number of monolayers in the electrodeposit which affect the surface activity, or the relevant surface-activity thickness (RSAT).

The first step in determining component activity coefficients is to choose a model for the molar excess Gibbs energy G^E. The excess properties are taken with reference to an ideal solution wherein the standard state for each component is the pure solid at the temperature and pressure of the mixture. Once the molar excess Gibbs energy is expressed, the activity coefficients γ_i can be found by (48)

$$RT \ln \gamma_i = \left(\frac{\partial (N_T G^E)}{\partial N_i} \right) . \qquad [24]$$

Since no general treatment has yet been developed to consider repulsion between ion cores or the interaction among cores and electrons at the Fermi surface, a useful approach is to treat the interaction between ions in a mixture by a pairwise model. The properties of such a system are represented by the sum of interactions between neighboring pairs of ion cores and the complications due to higher-order interactions are ignored. This quasichemical (or lattice theory) approach is outlined by Swalin (49) for regular solutions in which there is no excess entropy creation upon mixing, and any nonideality is considered in an enthalpy of mixing term. For the quasichemical approach, the activity coefficients for a binary, regular solution are given by (49,50)

$$\ln \gamma_A = \frac{(1 - x_A)^2 \Omega}{RT} \qquad [25]$$

$$\ln \gamma_B = \frac{(1 - x_B)^2 \Omega}{RT} \qquad [26]$$

where Ω is an adjustable parameter.

Equations [25] and [26] bear close resemblance to the two-suffix Margules equation. Guggenheim (51) has extended the quasichemical approach to model systems which exhibit considerable deviation from randomness. For this case, the excess entropy of mixing is no longer zero and a short-range order parameter is introduced which may be determined in some cases by x-ray and neutron diffraction techniques (49).

Two other informative treatments of solid-state thermodynamics should be mentioned before presenting the theoretical aspects for the activity model we have chosen to use in this paper. Darken and Gurry's text (52) contains a large number of references with tabular thermodynamic data for numerous metal systems, as well as an informative description of solid-state physical chemistry. Lumsden's (53) monograph illustrates the usefulness of thermodynamics for the accurate correlation of various equilibrium properties in alloy systems.

Electrodeposited metals usually have a more fine-grained, amorphous structure than their pyrometallurgical counterparts. Hence, the simple quasi-chemical lattice model does not generally represent the true thermodynamic nature of electrodeposited alloys. The activity model proposed by Renon and Prausnitz (54,55) is well suited to such a morphology. The authors define a local mole fraction x_{ij} representing the mole fraction of i in the vicinity of j. In a treatment similar to Guggenheim's extension of the quasichemical lattice theory, the local mole fractions are related to the overall mole fractions through Boltzmann factors:

$$\frac{x_{ji}}{x_{ki}} = \frac{x_j}{x_k} \frac{\exp(-\alpha_{ij} g_{ji}/RT)}{\exp(-\alpha_{ik} g_{ki}/RT)} \quad . \qquad [27]$$

The parameter α_{ij} ($\alpha_{ij} = \alpha_{ji}$) characterizes the tendency of components i and j to mix in a nonrandom fashion. The parameter g_{ik} ($g_{ik} = g_{ki}$) represents the energy of interaction between an $i-k$ molecular pair. Scott's theory (56) is used to relate the extensive excess properties to the interaction energies and the local mole fractions. For a solution of m components, the molar excess Gibbs energy is

$$\frac{G^E}{RT} = \sum_{i=1}^{m} x_i \frac{\sum_{j=1}^{m} \tau_{ji} G_{ji} x_j}{\sum_{k=1}^{i} G_{ki} x_k} \qquad [28]$$

where

$$\tau_{ji} = \frac{(g_{ji} - g_{ii})}{RT} \qquad [29]$$

and

$$G_{ji} = \exp(-\alpha_{ji} \tau_{ji}) \quad . \qquad [30]$$

Using Eqs. [24] and [28], the activity coefficient of component i can be calculated (54):

$$\ln \gamma_i = \frac{\sum_{j=1}^{m} \tau_{ji} G_{ji} x_j}{\sum_{k=1}^{m} G_{ki} x_k} + \sum_{j=1}^{m} \frac{x_j G_{ij}}{\sum_{k=1}^{m} G_{kj} x_k} \left(\tau_{ij} - \frac{\sum_{l=1}^{m} x_l \tau_{lj} G_{lj}}{\sum_{k=1}^{m} G_{kj} x_k} \right) . \qquad [31]$$

One of the advantages of this activity model is that it can be extended to as many components as desired without any additional assumptions and without adding any constants other than those obtained from binary data. This treatment is applicable to partially miscible as well as completely miscible systems.

Equilibrium-potential measurements of binary solids in contact with an aqueous phase containing the corresponding ions represent a convenient method for obtaining activity data. For some alloy systems, the simpler quasi-chemical treatment may represent the activity data quite well. This approach, outlined by Eqs. [25] and [26], can also be extended to model multicomponent systems. When Eqs. [25] and [26] cannot be used to fit the data, the computer programs listed in Appendix K of Ref. 57 can be used to fit the parameters of Eq. [31].

For this general treatment, we have chosen to use Eqs. [27]–[31] to describe the electrodeposit thermodynamics. However, the overall mole fractions in Eq. [27] must be adjusted to represent the surface, rather than bulk, composition. Though the activity model accounts for local composition, no characteristic length is associated with the range of applicability. Even for single-component electrodeposition systems, the surface plays a major role in the kinetics. Wranglen (58) observed that metals of low overvoltage grow by the lateral extension of layers, 0.1–1 μm thick. It was also observed that changing the current density changes the relative growth rates between crystal faces as well as where the deposited layers begin to grow on the respective crystal faces. Wranglen's microphotographic study of growth layers contains results for a periodic current source although no high-frequency results are reported.

Underpotential deposition studies can yield some information about the RSAT. Kolb et al. (59) correlated the underpotential shift between the bulk

deposit stripping peak and the first deposited monolayer stripping peak as a function of the difference in work functions between the substrate and the deposited material. The authors conclude that the work function of the first deposited monolayer may not differ greatly from that of the bulk electrodeposit, although the optical properties of such a monolayer are usually far from those of the bulk. Adzic et al. studied the underpotential deposition of Zn on Ag (60) and Zn on Cu and Au (61). For these reversible systems, the results support the work of Kolb et al. Approximately one monolayer of zinc was formed on the polycrystalline substrates prior to bulk deposition.

All of the work mentioned above indicates that the RSAT is about one monolayer. However, this may not be the case for all systems. Cadle and Bruckenstein (62) found that although only one monolayer of Bi is deposited on Pt by underpotential deposition, it is not until approximately 5 monolayers have been deposited that bulk deposition is occurring.

Takamura and Kozawa (63) have reviewed a great deal of literature concerned with the use of optical reflectance methods to investigate an electrode-electrolyte interface *in situ*. They have found that for a number of systems, the first few atomic layers do not have the same reflectance properties (64).

In general, higher current densities will shorten the RSAT. Setty and Wilman (65) have shown by electron diffraction experiments that high current densities promote the growth of a random, polycrystalline deposit growth which does not reflect the original electrode structure even during the initial stages of electrodeposition. Since most pulse-plating processes make use of unusually high current densities, a highly random (or amorphous), polycrystalline deposit typically results. It has also been observed that the influence of a polycrystalline substrate with small crystallite grains ceases to exist at much earlier stages of deposition than that of the surface of a large single crystal substrate (66).

Though there is a wealth of literature concentrating on epitaxy and morphology of electrodeposits, there is no clear *a priori* approach to estimate the

RSAT. The work reviewed in this paper dealt only with the early stages of electrodeposition. In a pulse-plating processes, the deposit usually has a random, polycrystalline structure, and the RSAT is probably much less than that of the initially deposited monolayer.

Optical studies seem to indicate that the RSAT can be greater than a monolayer. Conversely, the high current-density pulses often used in practical plating operations may lower the RSAT to about a monolayer. In light of the above considerations, it may be advantageous to weight the substrate's influence on the newly forming surface with a function that decays with depth (67,68). For the purposes of this work, the following heuristic treatment will be used in estimating a relevant surface composition x_i:

$$x_i = \frac{\sum_{ml} \left[1 - \exp\left(-\sigma \frac{RSAT - d_{ml}}{RSAT} \right) \right] x_{i,ml}}{\sum_{ml} \left[1 - \exp\left(-\sigma \frac{RSAT - d_{ml}}{RSAT} \right) \right]} \qquad [32]$$

where $d_{ml} \leq RSAT$.

In Eq. [32], the subscript ml refers to a monolayer, d_{ml} is the monolayer's distance from the surface, σ is a system-specific proportionality constant, $x_{i,ml}$ refers to the monolayer mole fraction of component i, and the bracketed terms are weighting functions for each monolayer. Monolayers that are deep below the surface make only a small contribution to the relevant surface composition. For $d_{ml} > RSAT$, no effect on the surface composition is taken in account. Equation [32] assures that the sum of the overall mole fractions is unity. It can also be seen that if σ is set to a very high value, then the weighting function for each monolayer within the RSAT will essentially be unity.

We can now formalize in the following algorithm the procedure for the implementation of the mathematical model.

For $t = t_1, t_2, \cdots t_n$

1. Obtain the total current i_n.
2. Solve for $\Theta^s_{i,n}$ and $\Psi^s_{i,n}$ (Eqs. [12]–[15]).
3. Solve for H_n (Eq. [21]).
4. Solve for $(\partial H_n/\partial E_n)$ (Eq. [23]).
5. Solve for E_n by iteration (Eq. [22]).
6. Obtain the new surface composition from the individual currents according to Faraday's law (Eqs. [18] and [32]).
7. Determine the new surface activity (Eq. [31]).

Results

Table 1 lists the values of most of the variables used in this treatment. For the base case, the current is pulsed to the total dc limiting current of the system. This current program is displayed in Fig. 1. In Fig. 2, the dimensionless surface concentrations are plotted for a system in which a Nernst diffusion layer is applicable (the dotted curves) and for the more rigorous solution outlined by Eqs. [12] and [13] (the unbroken curves). It can be seen that the two solution techniques yield very similar answers, as would be expected from the close agreement of the respective current-step solutions. Due to the low bulk concentration and more noble character of component one, its surface concentration remains negligible throughout the electrodeposition process. The least noble component 3 has the highest bulk and surface concentration. Figure 2 illustrates that the process reaches a uniform and sustained periodic state after about the fourth cycle.

The electrode-potential profile is portrayed in Fig. 3. The lower portions of the curve correspond to the on-time. While deposition is occurring, the electrode potential is forced to more cathodic (negative) values since the discharging ion concentrations are decreasing. During the off-times, the potential drifts in the anodic direction as corrosion reactions take place and metal ions are tran-

sported to the electrode surface by convection and diffusion.

One of the more practical aims of this work is to obtain the electrodeposit composition. A plot of the deposit composition is shown in Fig. 4. Though component 1 is the most noble component, its low bulk concentration limits its rate of mass transfer thereby suppressing its deposit concentration. The opposite is true for component 3. About 10 monolayers are deposited during the on-time; thus, there is a considerable variation in the electrodeposit concentration during the on-time. The corrosion currents also cause a change in the deposit mole fractions during the off-time. At higher frequencies, there would be less variation in the deposit composition during a pulse.

In order to obtain the deposit mole fractions, the partial currents must be known. A plot of partial currents is shown in Fig. 5 for a pulse-reversal current source. A pulse-reversal current source is often used to produce smooth deposits, and it has a significant affect on the alloy composition and ionic surface concentrations. Due to the high bulk concentration of component 3, it carries most of the cathodic current. Figure 5 shows that components 1 and 2 incur mass-transport limitations during the on-time. Component 3 also carries most of the anodic current due to its more negative standard electrode potential. At the end of the fifth cycle, the total deposit mole fractions are 0.028, 0.222, and 0.750 for components 1, 2, and 3, respectively. For the base case (Figs. 1–4) the analogous values are 0.021, 0.175, and 0.804. In addition, the pulse-reversal current source supports higher ionic surface concentrations due to the periodic deposit dissolution. A comparison of Figs. 2 and 6 illustrates this.

Some insight into multicomponent electrodeposition can be gained by examining the case of a triangular current source. The triangular current waveform in Fig. 7 reaches a cathodic current density 1.7 times the total dc limiting current density displayed in Fig. 1. The nonlinear nature of the electrode kinetics is manifest in the electrode-potential profile in Fig. 8. The waveform in Fig. 7 was constructed to disallow the achievement of a periodic state. In Fig. 8, it can

be seen that the minima reach more cathodic values for each succeeding period. At 0.20 sec, all three discharging metal ions reach a zero surface concentration. Directly after this another reaction would be forced to take place, such as solvent decomposition.

The influence of the individual solid-state activities is shown by the comparison of Figs. 9 and 10 for the last off-time displayed in Fig. 1. The partial currents for the base case are shown in Fig. 9. Component 1 carries its dc limiting current density throughout the process. Component 2 is also depositing during the off-time whereas component 3 dissolves. The partial currents sum to zero during the off-time.

When the energy of interaction between components 1 and 3 and components 2 and 3 is attractive, the corrosion currents are reduced and the deposit is more stable during the off-time. This is depicted in Fig. 10. These concepts are important to the understanding of the corrosion of alloys. In particular, elements can be chosen to form a more corrosion resistant alloy. Though the partial currents are relatively low in Figs. 9 and 10, and the overall deposit composition will not change greatly because of the surface free-energy changes, situations can occur in which the individual solid-state activities could be very important. For instance, in pulse-reversal electrodeposition, where the magnitude of the anodic current is high, the surface activities will play an important role in determining the electrodeposit composition and the ionic surface concentrations.

Conclusions

This paper presents a mathematical model for the periodic electrodeposition of multicomponent alloys by an arbitrarily specified current source. An analogous model for potential-controlled electrolysis is also discussed. The method of superposition is used to solve this problem with an efficient numerical algorithum. This treatment exposes the large number of parameters the electroplater must consider for obtaining thin alloy films with the desired proper-

ties. If an accurate model is used by the electroplater, the different plating parameters can be intelligently varied to assist in manufacturing the desired electrodeposit.

Acknowledgement

Our modeling efforts were benefited by insightful discussions with Professor John Newman.

This work was supported by the Director, Office of Energy Research, Office of Basic Energy Sciences, Materials Sciences Division of the Office of the U.S. Department of Energy, under Contract No. DE-AC03-76SF00098.

Appendix

Roseburgh and Lash Miller's solution could be used to derive alternate expressions for Eqs. [12] and [13]. The current-step solution is first required. Fick's second law,

$$\frac{\partial c_i}{\partial t} = D_i \frac{\partial^2 c_i}{\partial y^2} \quad , \qquad \text{[A-1]}$$

with the initial condition and the boundary conditions given by Eqs. [3], [5], and [10] outline the current-step problem. The solution is (23)

$$c_i = c_i^b + \frac{i_i \delta_i}{n_i F D_i}\left[1 - \frac{y}{\delta_i} - \frac{8}{\pi^2}\sum_{j=1}^{g} \frac{\cos(mg_i y)}{m^2} e^{-m^2 \alpha_i t}\right] \qquad \text{[A-2]}$$

where $m = 2j - 1$, $g_i = \pi/2\delta_i$, and $\alpha_i = \pi^2 D_i/4\delta_i^2$.

The similarity between Eqs. [7] and [A-2] is evident. Retention of the velocity term in Eq. [1], the convective diffusion equation, tends to change slightly the eigenfunctions and the eigenvalues. The form and the behavior of the two current step solutions are very similar.

For short times, Eq. [A-2] can be reduced to the Sand equation. Thus, Eq. [8] bears a close resembiance to the asymptotic expression of Eq. [A-2] evaluated for short times and at the electrode surface.

When the method of superposition is used to obtain an expression for a varying current source, the concentration can be expressed by Eq. [11] and

$$\Theta_{i,n} = \frac{\delta_i}{n_i F D_i}\left[1 - \frac{y}{\delta_i} - \frac{8}{\pi^2}\sum_{j=1}^{\infty} \frac{\cos(mg_i y) e^{-m^2 \alpha_i (t - t_n - 1)}}{m^2}\right] \qquad \text{[A-3]}$$

and

$$\Psi_{i,n} = c_i^b + \frac{\delta_i}{n_i F D_i}\left\{\frac{8}{\pi^2}\sum_{j=1}^{n-1} i_{i,j} \sum_{k=1}^{\infty} \frac{\cos(mg_i y)}{m_2}\left[e^{-m^2 \alpha_i (t - t_k)} - e^{-m^2 \alpha_i (t - t_{k-1})}\right]\right\} . \qquad \text{[A-4]}$$

The similarity between Eqs. [12], [13], [A-3], and [A-4] is evident. This is especially true at the electrode surface where Z_k is unity. Equations [A–3] and

[A–4] and Eqs. [14] and [15] were used to model the solution-side mass transport in order to obtain the dotted curves in Fig. 2.

Nomenclature

$a_{i,n}$	surface activity of component i at time step n
$c_{i,n}$	concentration of species i during time step n, mol/cm^3
c_i^b	bulk concentration of species i, mole/cm^3
$c_{i,n}^s$	surface concentration of species i during time step n, mole/cm^3
$c_{i,re}$	reference electrode compartment concentration of species i, mole/cm^3
d_{ml}	monolayer thickness of electrodeposit, cm
D_i	diffusion coefficient of species i, cm^2/sec
f	F/RT, mole/V-equivalent
F	Faraday's constant, 96487 C/equivalent
g_{ij}	energy of interaction between components i and j, J/mole
G^E	molar excess Gibbs energy, J/mole
H_n	zeroing function, mA/cm^2
$i_{i,n}$	current density carried by species i at time step n, mA/cm^2
i_n	total current density at time step n, mA/cm^2.
$k_{a,i}$	anodic rate constant of component i, mole/cm^2–sec
$k_{c,i}$	cathodic rate constant of species i, kg/cm^2–sec
m	number of deposit components
M_i	symbol for chemical formula of species i
n	time step
n_i	number of electrons in the deposition reaction of species i
n_{re}	number of electrons in reference-electrode reaction
N_i	moles of component i
N_T	total moles

r	cell ohmic resistance, Ω–cm^2
R	universal gas constant, 8.314 J/mole-K
RSAT	relevant surface-activity thickness, cm
$s_{i,re}$	stoichiometric coefficient of species i in reference electrode reaction
t	time, sec
T	absolute temperature, K
U_i^θ	standard electrode potential for reaction involving species i, V
U_{re}^θ	standard electrode potential of the reference electrode reaction, V
V_n	electrode potential referred to the reference electrode, during time step n, V
v_y	normal velocity component to a rotating disk electrode, cm/sec
x_i	mole fraction of component i
y	normal distance from the electrode surface, cm
α_{ij}	species interaction constant characteristic of the nonrandomness of the mixture
β_i	symmetry factor for component i
γ_i	activity coefficient of component i
$\Gamma(4/3)$	0.89298, the gamma function of 4/3
$\Theta_{i,n}$	concentration function, mole/A-cm
$\Theta_{i,n}^s$	surface-concentration function, mole/A-cm
δ_i	Nernst diffusion layer thickness of species i, cm
σ	exponential proportionality constant for the RSAT mole fraction
ν	kinematic viscosity, cm^2/sec
ρ_o	solvent mass density, kg/cm^3

ρ_i	species i molar density, moles/cm^3
ω	disk rotation speed, radian/sec
$\Psi_{i,n}$	concentration function, mole/cm^3
$\Psi^s_{i,n}$	surface concentration function, mole/cm^3

References

1. A. Brenner, *Electrodeposition of Alloys, Principles and Practice*, Academic Press, New York, 1963.
2. K.M. Gorbunova and Yu.M. Polukarov, *Advances in Electrochemistry and Electrochemical Engineering*, Vol. 5, C.W. Tobias, Editor, Interscience, New York, 1967, p. 256.
3. C.C. Wan, H.Y. Cheh, and H.B. Linford, *Plating*, 61 (1974) 559.
4. A.J. Avila and M.J. Brown, *Plating*, 57 (1970) 1105.
5. H.Y. Cheh, *J. Electrochem. Soc.*, 118 (1971) 551.
6. V.A. Lamb, *Plating*, 56 (1969) 909.
7. J. Cl. Puippe and N. Ibl, *Plating*, 67 (1980) 68.
8. A.R. Despic and K.I. Popov, *J. Appl. Electrochem.*, 1 (1971) 275.
9. K.I. Popov, *Modern Aspects of Electrochemistry*, No. 7, B.E. Conway and J. O'M. Bockris, Editors, Plenum Press, New York, 1972, p. 304.
10. W. Sullivan, *Plating*, 62 (1975) 139.
11. M.H. Gelchinski, L. Gal-Or, and J. Yahalom, *J. Electrochem. Soc.*, 129 (1982) 2433.
12. C.A. Burrus, *J. Electrochem. Soc.*, 118 (1971) 833.
13. H. Leidheiser, Jr. and A.R.P. Ghuman, *ibid*, 120 (1973) 484.
14. U. Cohen, F.B. Koch, R. Sard, *ibid*, 130 (1983) 1987.
15. A. Kindler, *Ph.D. Thesis*, University of California, Berkeley (1981).
16. N. Ibl and K. Schadegg, *J. Electrochem. Soc.*, 114 (1967) 54. D.T. Chin, *ibid*, 130 (1983) 1657.
17. D.T. Chin, *ibid*, 130 (1983) 1657.
18. K. Niscancioglu, *Ph.D. Thesis*, University of California, Berkeley (1973).

19. R. Haynes, *ibid*, 126 (1979) 881.

20. P. Radhakrishnamurty, *ibid*, 127 (1980) 1320.

21. R. Haynes, *ibid*, 127 (1980) 1321.

22. H.Y. Cheh, *ibid*, 127 (1980) 1321.

23. T. Cheng and H.Y. Cheh, 161'st Electrochemical Society Meeting, Abstract No. 414, Montreal, Canada, 1982.

24. T. Cheng and H.Y. Cheh, 164th Electrochemical Society Meeting, Abstract No. 249, Washington, DC, 1683.

25. W.G. Cochran, *Proceeding of the Cambridge Philosophical Society*, 30 (1934) 365.

26. J.S. Newman, *Electrochemical Systems*, Prentice-Hall, Inc., Englewood Cliffs, NJ, 1973.

27. J.S. Newman, *J. Electrochem. Soc.*, 113 (1966) 1235.

28. J.S. Newman, *ibid.*, 117 (1970) 198.

29. P. Appel, Ph.D. Thesis, University of California, Berkeley (1976).

30. V.S. Krylov and V.N. Babak, *Sov. Electrochem.*, 7 (1971) 626.

31. D.A. Scherson, P.F. Marconi, J.S. Newman, *J. Electrochem. Soc.*, 127 (1980) 2603.

32. K. Niscancioglu and J.S. Newman, *J. Electroanal. Chem.*, 50 (1974) 23.

33. V.G. Levich, *Physiochemical Hydrodynamics*, Prentice-Hall, Englewood Cliffs, NJ, 1961, p. 69.

34. T.R. Roseburgh and W. Lash Miller, *J. Phys. Chem.*, 14 (1970) 816.

35. H.Y. Cheh, *J. Electrochem. Soc.*, 118 (1971) 1132.

36. K. Visawanathan and H.Y. Cheh, *ibid*, 125 (1978) 1616.

37. K. Visawanathan and H.Y. Cheh, *J. Appl. Electrochem.*, 9 (1979) 537.

38. J.M. Hale, *J. Electroanal. Chem.*, 6 (1963) 187.

39. Yu.G. Siver, *Russ. J. Phys. Chem.*, 34 (1960) 274.

40. K. Visawanathan, M.A. Farrell, and H.Y. Cheh, *J. Electrochem. Soc.*, 125 (1978) 1772.

41. P.C. Andricacos and H.Y. Cheh, *J. Electroanal. Chem.*, 121 (1981) 133.

42. W.M. Kays and M.E. Crawford, *Convective Heat and Mass Transfer*, McGraw Hill Book Company, 1980, p. 117–129.

43. F.B. Hildebrand, *Advanced Calculus for Applications*, Prentice-Hall, Inc., Englewood Cliffs, New Jersey, 1976, 463–467.

44. M. Fleischmann and H.R. Thirsk, *Advances in Electrochmistry and Electrochemical Engineering*, Vol. 3, P. Delahay, Editor, Interscience, New York, 1963, p. 124.

45. K.J. Vetter, *Electrochemical Kinetics*, S. Bruckenstein and B. Howard, Translaticn Editors, Academic Press, New York, 1967, p. 140.

46. L. Lapidus, *Digital Computation for Chemical Engineers*, McGraw-Hill Book Company, 1962, p. 288.

47. R.C. Alkire and J.E. Tsai, *J. Electrochem. Soc., 129 (1982) 1157.*

48. E.A. Guggenheim, *Thermodynamics*, North-Holland Publishing Company, Amsterdam, 1959, p. 215.

49. R.A. Swalin, *Thermodynamics of Solids*, John Wiley and Sons, 1972, p. 141–153.

50. J.M. Prausnitz, *Molecular Thermodynamics of Fluid-Phase Equilibria*, Prentic-Hall, Inc., Englewood Cliffs, NJ, p. 279–292.

51. E.A. Guggenheim, *Mixtures*, Oxford Press, London, 1952, p. 215–242.

52. L.S. Darken and R.W. Gurry, *Physical Chemistry of Metals*, R.F. Mehl, consulting editor, McGraw-Hill Book Company, Inc., 1953.

53. J. Lumsden, *Thermodynamics of Alloys*, Institute of Metals, London, 1952.

54. H. Renon and J.M. Prausnitz, *A.I.Ch.E.J.*, 14 (1968) 135.

55. J.M. Prausnitz, *op. cit.*, p. 309–314.

56. R.L. Scott, *J. Chem. Phys.* 25 (1956) 193.

57. Renon, H.M., Ph.D. Thesis, University of California, Berkeley (1966).

58. Wranglen, *Electrochem. Acta*, 2 (1960) 130.

59. D.M. Kolb, M. Prazasnyski, H. Gerischer, *J. Electroanal. Chem.*, 54 (1974) 25.

60. G. Azdic, J. McBreen, and M.G. Chu, *J. Electrochem. Soc.*, 128 (1981) 1691.

61. J. McBreen, M.G. Chu, G. Azdic, *ibid*, 128 (1981) 2281.

62. S.H. Cadle and S. Bruckenstein, *Anal. Chem.*, 44 (1974) 1993.

63. T. Takamura and K. Takamura, *Surface Electrochemistry, Advanced Methods and Concepts*, Japan Scientific Societies Press, T. Takamura and A. Kozawa, Editors, p. 222–234.

64. T. Takamura, F. Watanabe, and K. Takamura, *Electrochem. Acta*, 19 (1974) 933.

65. T.H.V. Setty and H. Wilman, *Trans. Faraday Soc.*, 51 (1955) 984.

66. J.O'M. Bockris and A. Damjanovic, *Modern Aspects of Electrochemistry*, No. 3, J.O'M. Bockris and B.E. Conway, Editors, Butterworth and Co. LTD, London, p. 329.

67. K.H.Z. Brainina, D.P. Synkova, and I.G. Yudelevich, *J. Electroanal. Chem.*, 35 (1972) 165.

68. K.H.Z. Brainina, N.K. Kiva, and V.B. Beliavskaia, *Electrokhimiya*, 1 (1965) 311.

Table 1. Model inputs.[1]

Quantity				Units
c_i^b	1×10^{-6}	1×10^{-5}	1×10^{-4}	mole/cm^3
d_m	3			Å
$k_{a,i}$	8.741×10^{-14}	2.109×10^{-10}	5.091×10^{-7}	mole/cm^2–s
$k_{c,i}$	1.229×10^{-3}	5.092×10^{-7}	2.110×10^{-10}	kg/cm^2–s
n_i	2	2	2	---
r	0			ohm-cm^2
RSAT	9			Å
U_i^{θ}[2]	0.3	0.1	−0.1	Volts
x_i^o	1.0	0.0	0.0	moles i/mole
β_i	0.5	0.5	0.5	---
γ_i	1.0	1.0	1.0	---
δ_i	0.001014	0.001014	0.001014	cm
ρ_o	0.001			kg/cm^3
ρ_i	0.073	0.073	0.073	mole/cm^3
σ	1.0			---

[1]For component entries, component 1 is at the far left, followed by components 2 and 3 respectively.
[2]The values of U_i^{θ} can be obtained from the rate constants.
The rate constants have been chosen to yield comparable exchange current densities.

Figure Captions

Fig. 1. Current source for the base case. The maximum cathodic current is the sum of the dc limiting currents of the discharging ions (−211 mA/sq·cm).

Fig. 2. Dimensionless surface concentrations for the first five cycles. The current source is shown in Fig. 1. The dotted curve was obtained using the Nernst diffusion layer approximation. The surface concentration of component 1 remains near zero throughout the deposition process.

Fig. 3. Electrode potential relative to a SHE for the base case. The lower portion of the curve represents the on-time.

Fig. 4. RSAT mole fraction variation for the base case. Upper curve, component 3; middle curve, component 2; lowest curve, component 1. At time zero, the electrode is pure 1.

Fig. 5. Component currents for a pulse-reversal current source. The current is reversed to 52.8 mA/sq·cm. The maximum cathodic current is the same as that shown in Fig. 1 (211.2 mA/sq·cm).

Fig. 6. Dimensionless surface concentrations for the pulse-reversal current source. The surface concentrations are higher than those for the pulsed-current source depicted in Fig. 2.

Fig. 7. Triangular current source. The maximum current is 1.6 times the base case maximum cathodic current source shown in Fig. 1.

Fig. 8. Electrode potential relative to the SHE for the triangular current source displayed in Fig. 7. For the specified conditions, a periodic state will not be achieved.

Fig. 9. Component currents during the fifth off-time for the base case. The activity coefficients are all unity.

Fig. 10. Component currents during the fifth off-time of the current source shown in Fig. 2. For this case, the activity coefficients deviate from unity. $G_{3,1} - G_{3,3} = G_{3,2} - G_{3,3} = -20{,}000$ J/mole. Component 3 is attracted to components 1 and 2 in the electrodeposit.

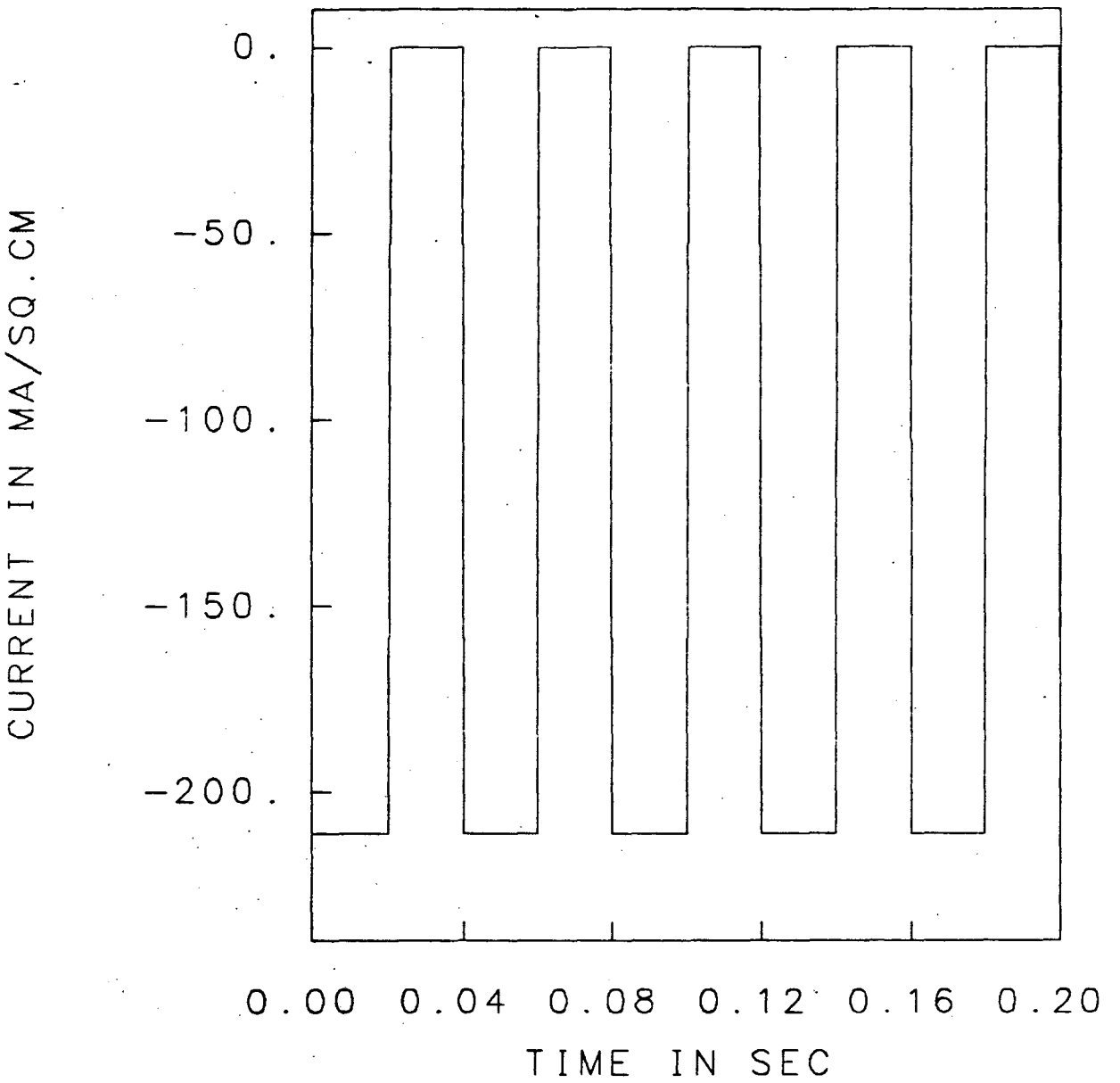
0.
-50.
-100.
-150.
-200.
CURRENT IN MA/SQ.CM
0.00
0.04
0.08
0.12
0.16
0.20
TIME IN SEC

Fig. 1

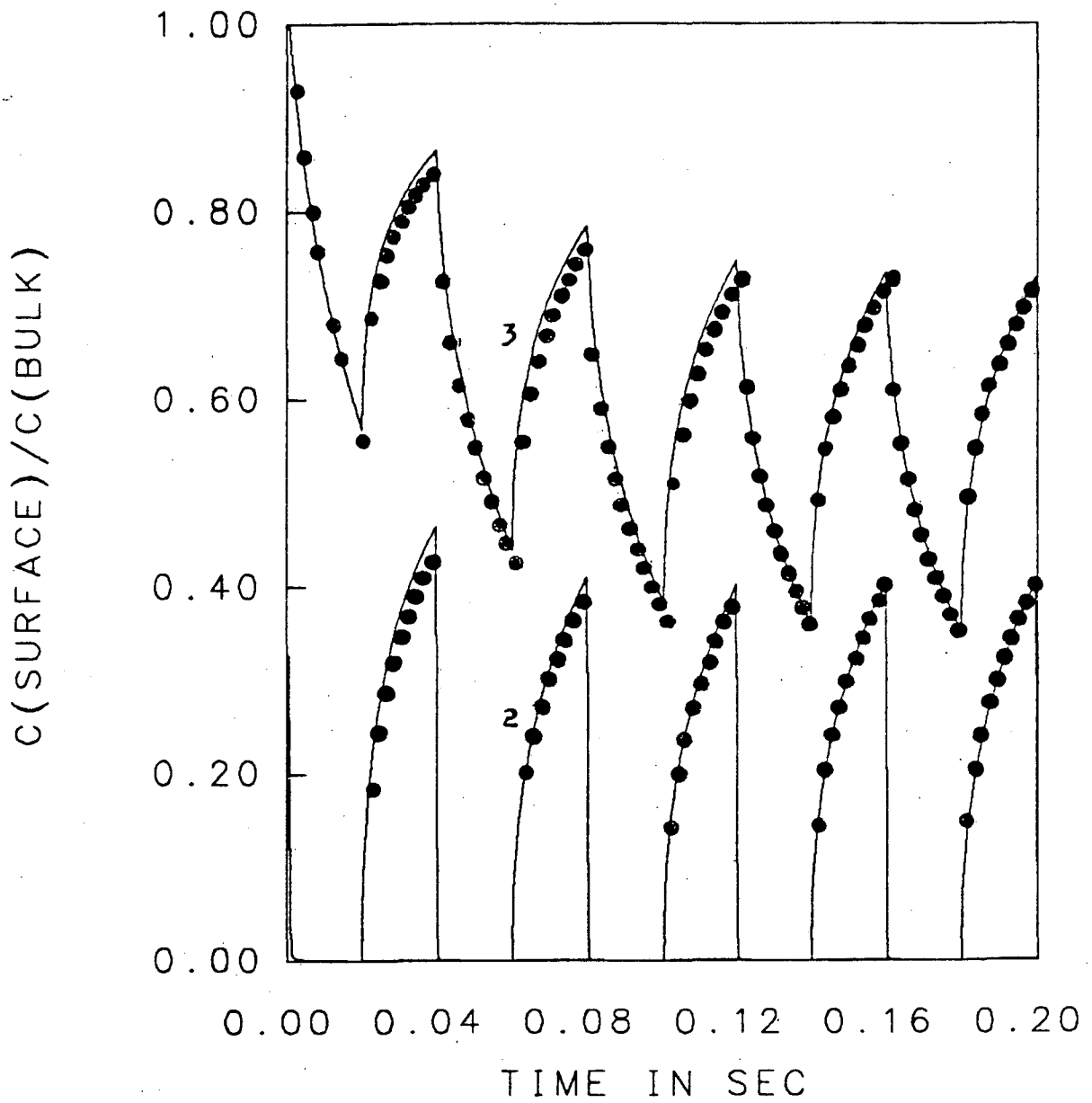
1.00
0.80
0.60
0.40
0.20
0.00
C(SURFACE)/C(BULK)
3
2
0.00
0.04
0.08
0.12
0.16
0.20
TIME IN SEC

Fig. 2

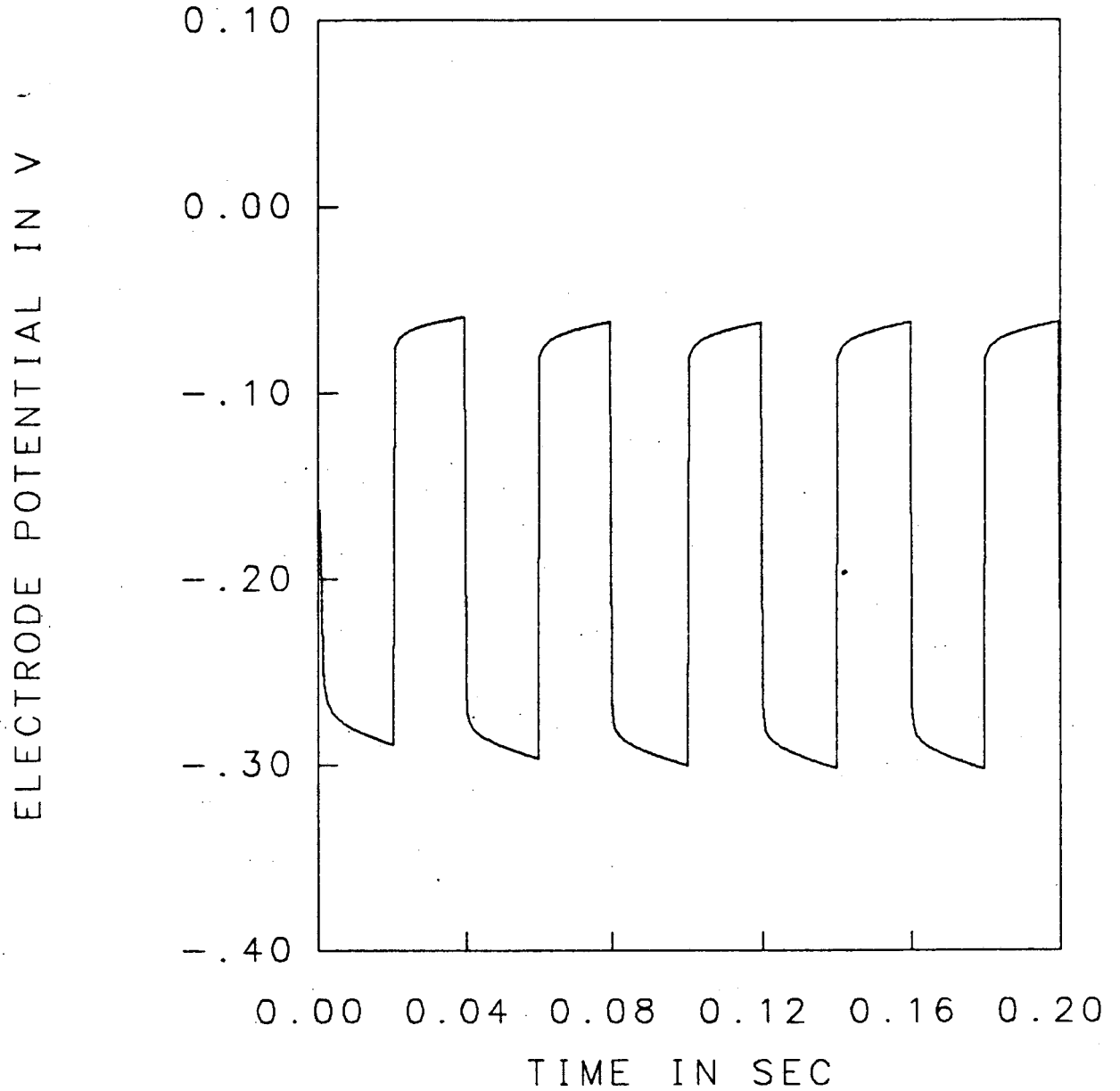
0.10
0.00
-.10
-.20
-.30
-.40
ELECTRODE POTENTIAL IN V
0.00
0.04
0.08
0.12
0.16
0.20
TIME IN SEC

Fig. 3

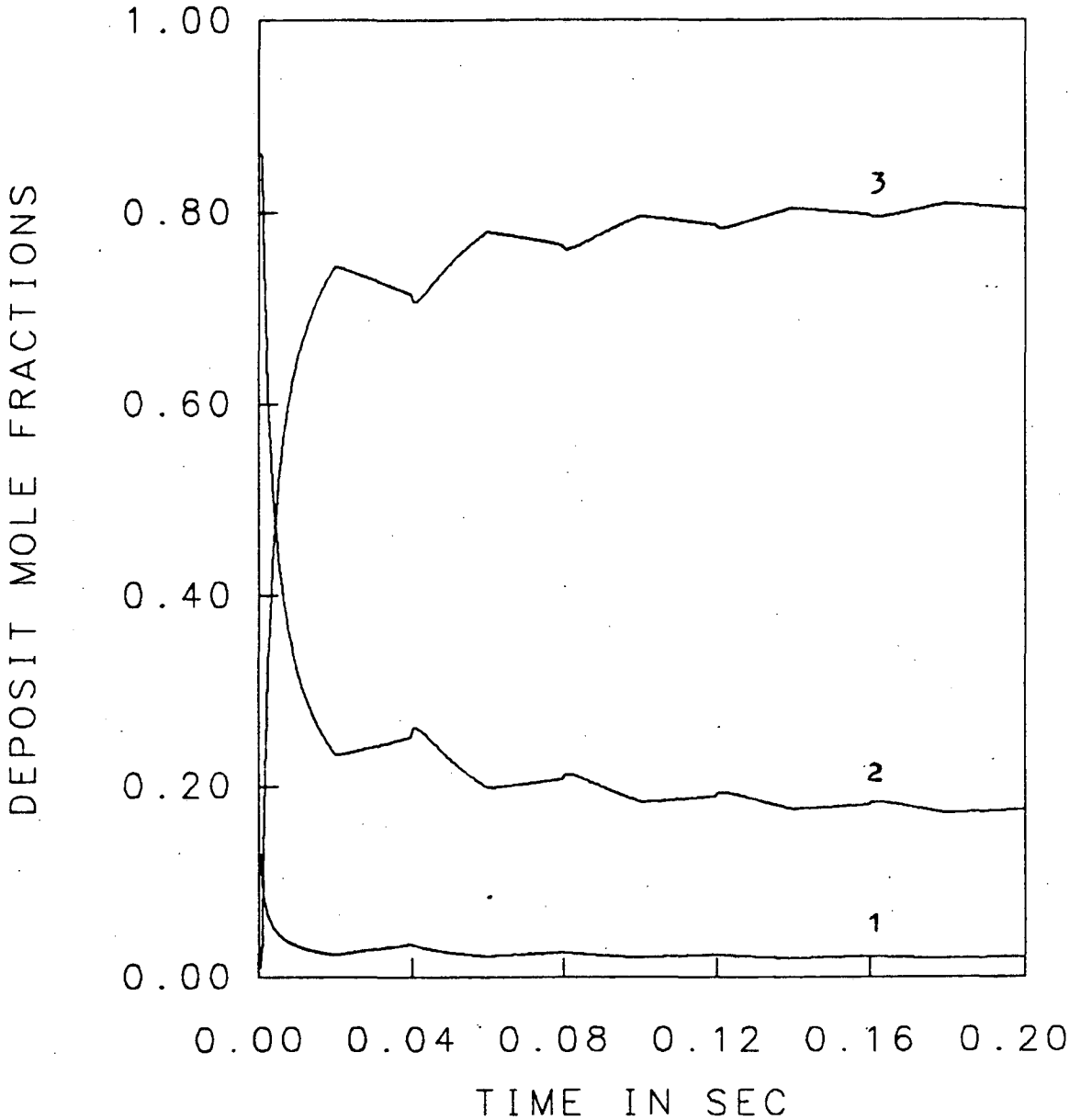
1.00
0.80
0.60
0.40
0.20
0.00
DEPOSIT MOLE FRACTIONS
3
2
1
0.00
0.04
0.08
0.12
0.16
0.20
TIME IN SEC

Fig. 4

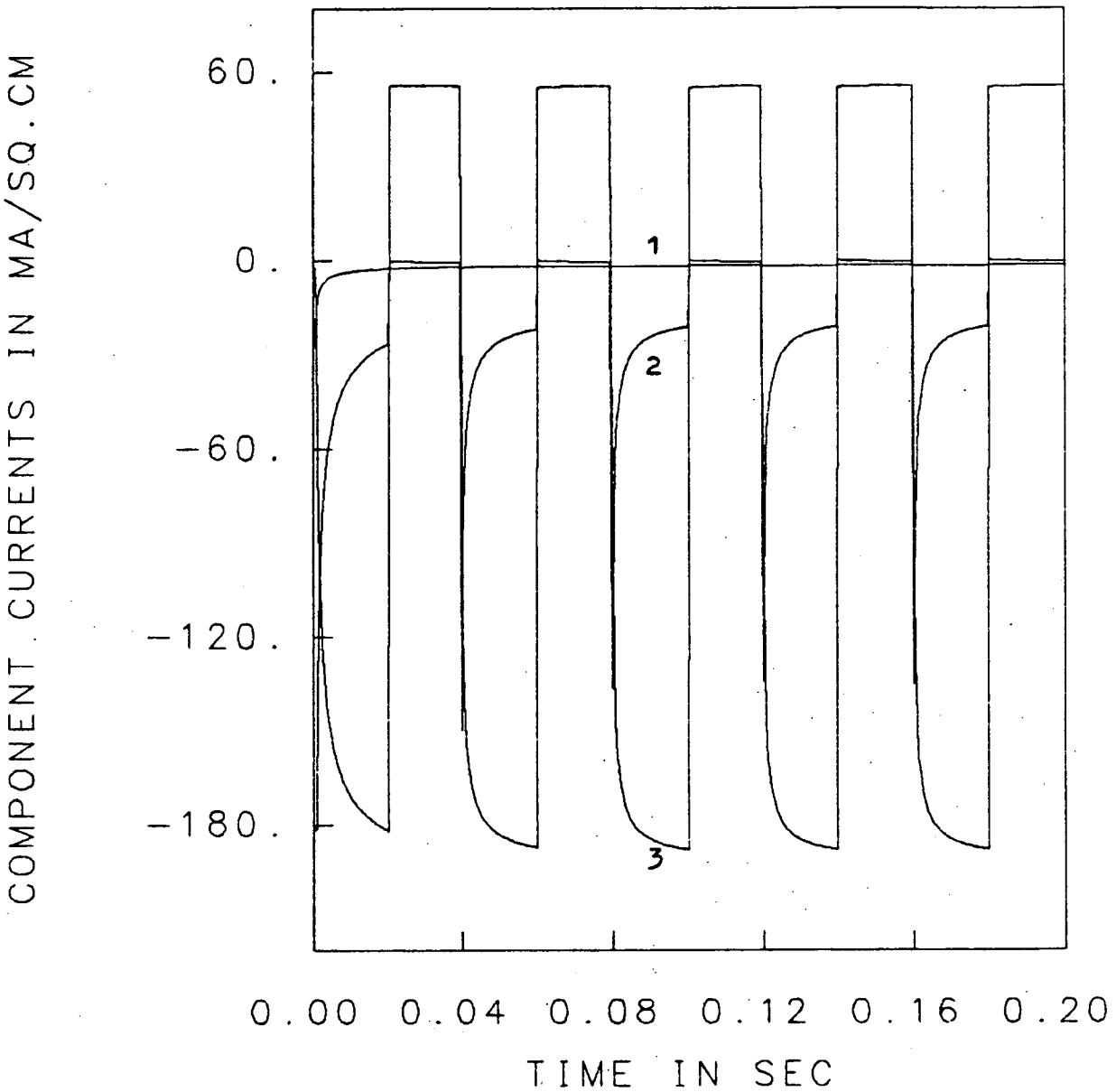
COMPONENT CURRENTS IN MA/SQ.CM
60.
0.
-60.
-120.
-180.
1
2
3
0.00
0.04
0.08
0.12
0.16
0.20
TIME IN SEC

Fig. 5

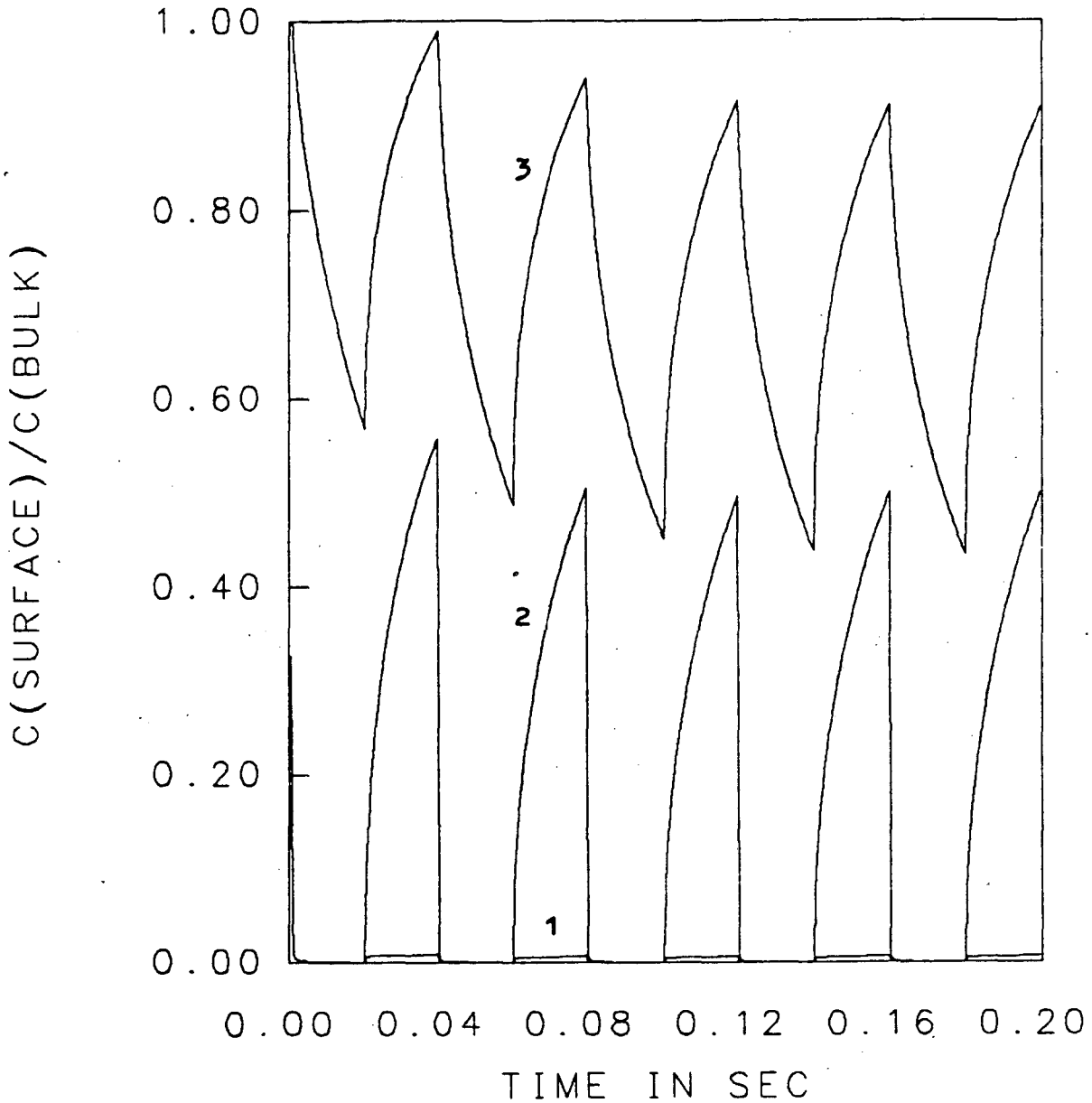
1.00
0.80
0.60
0.40
0.20
0.00
C(SURFACE)/C(BULK)
3
2
1
0.00
0.04
0.08
0.12
0.16
0.20
TIME IN SEC

Fig. 6

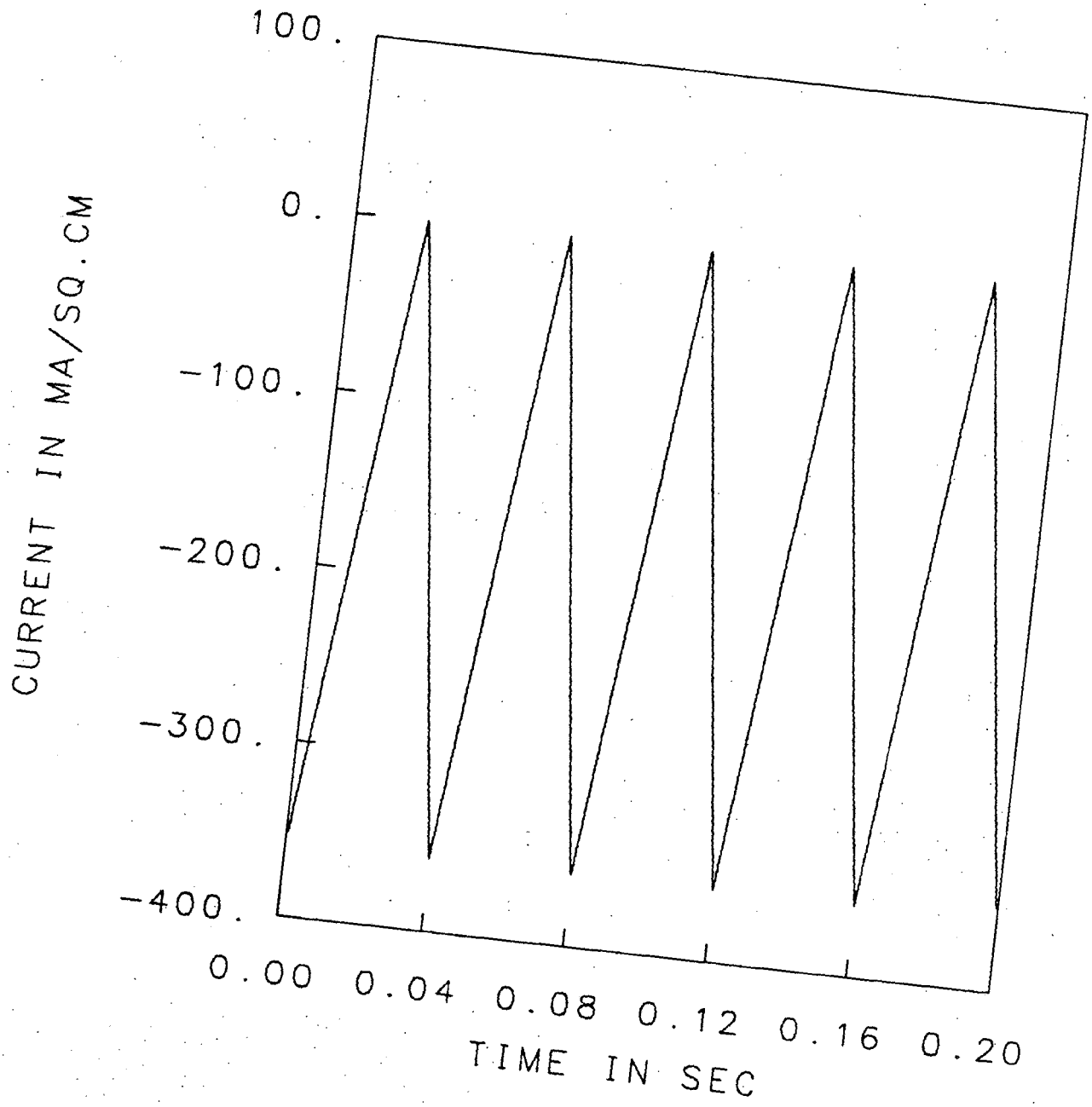
100.
0.
-100.
-200.
-300.
-400.
CURRENT IN MA/SQ.CM
0.00
0.04
0.08
0.12
0.16
0.20
TIME IN SEC

Fig. 7

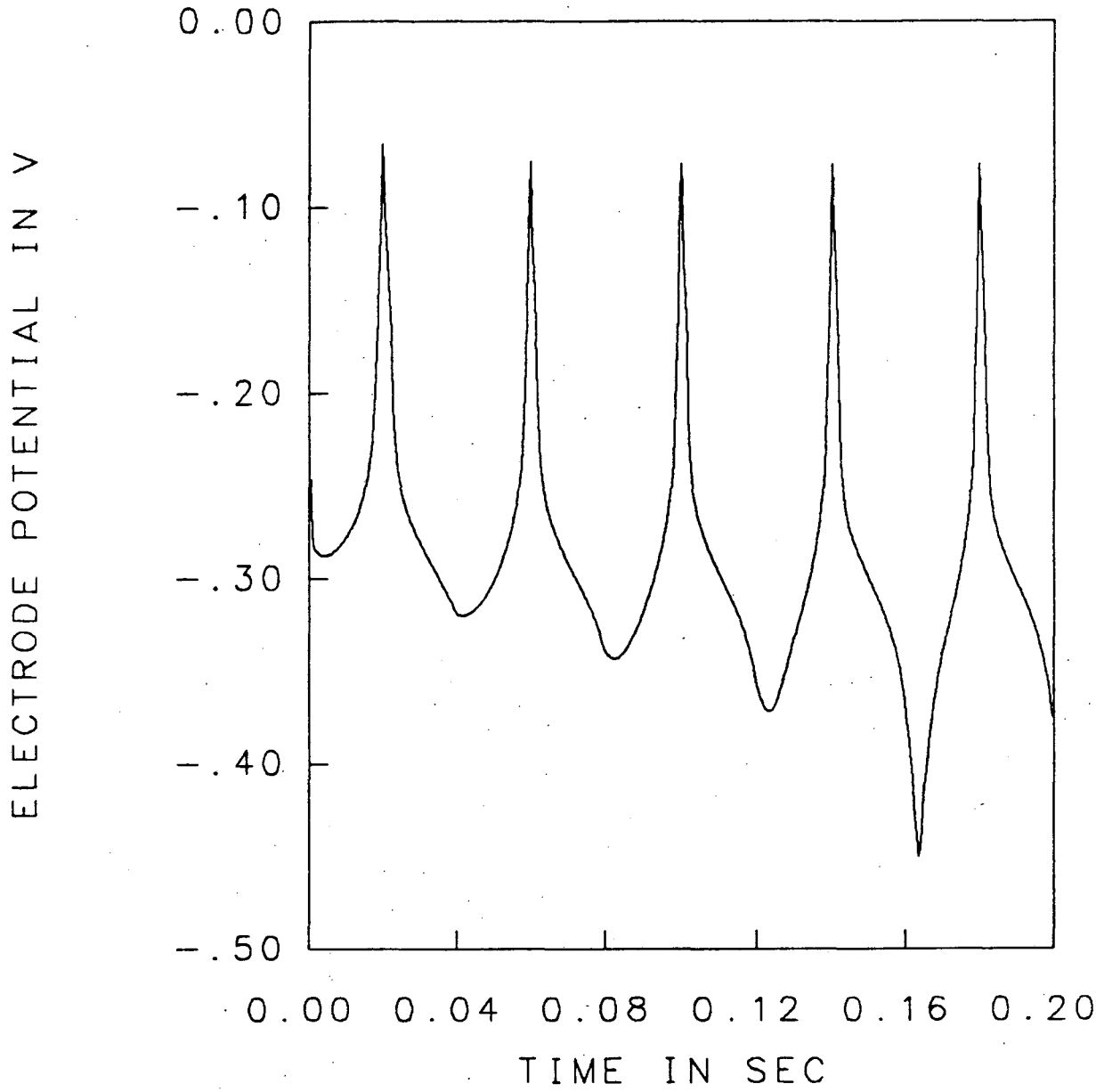
0.00
-.10
-.20
-.30
-.40
-.50
ELECTRODE POTENTIAL IN V
0.00
0.04
0.08
0.12
0.16
0.20
TIME IN SEC

Fig. 8

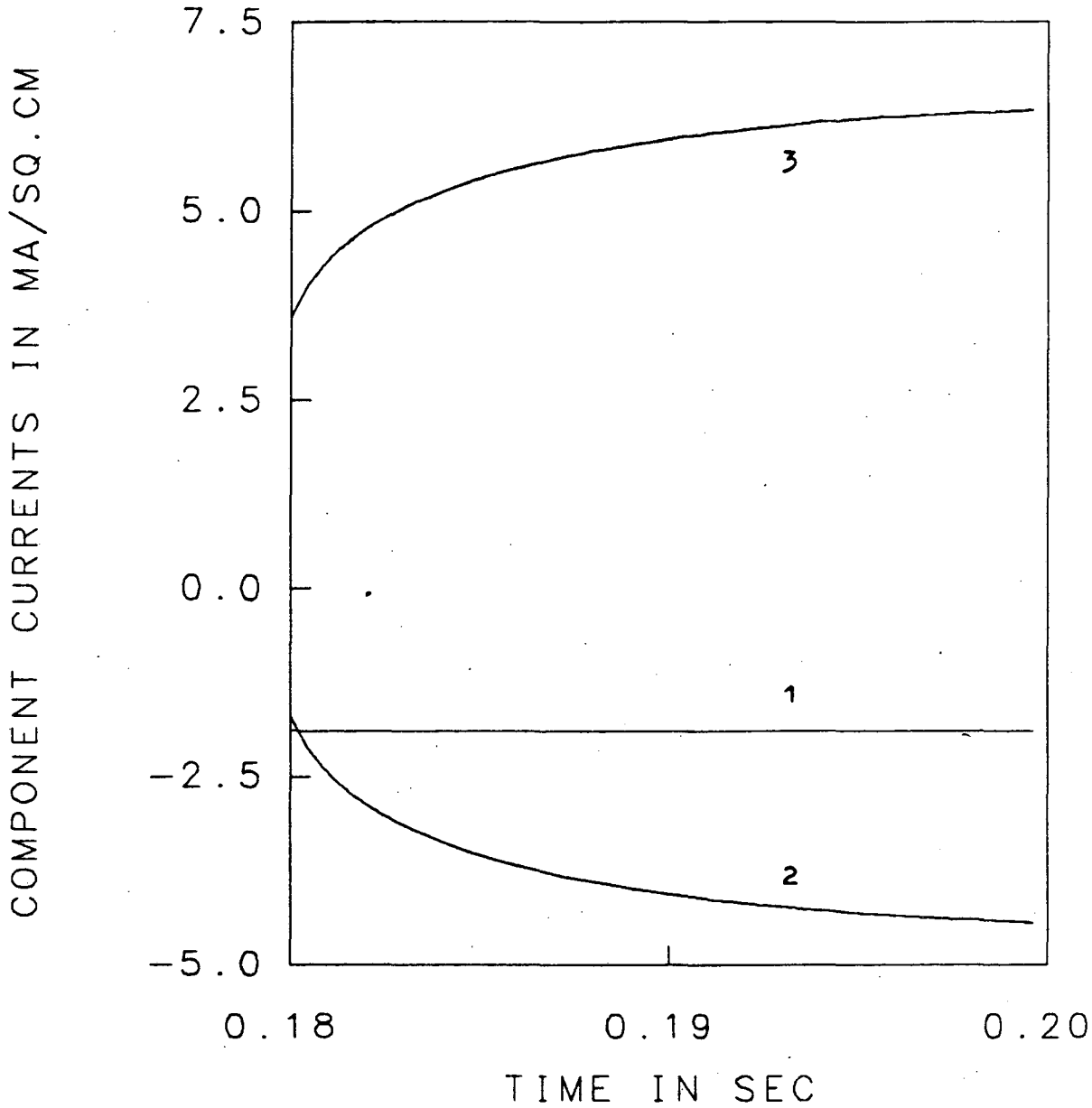
7.5
5.0
2.5
0.0
-2.5
-5.0
COMPONENT CURRENTS IN MA/SQ.CM
3
1
2
0.18
0.19
0.20
TIME IN SEC

Fig. 9

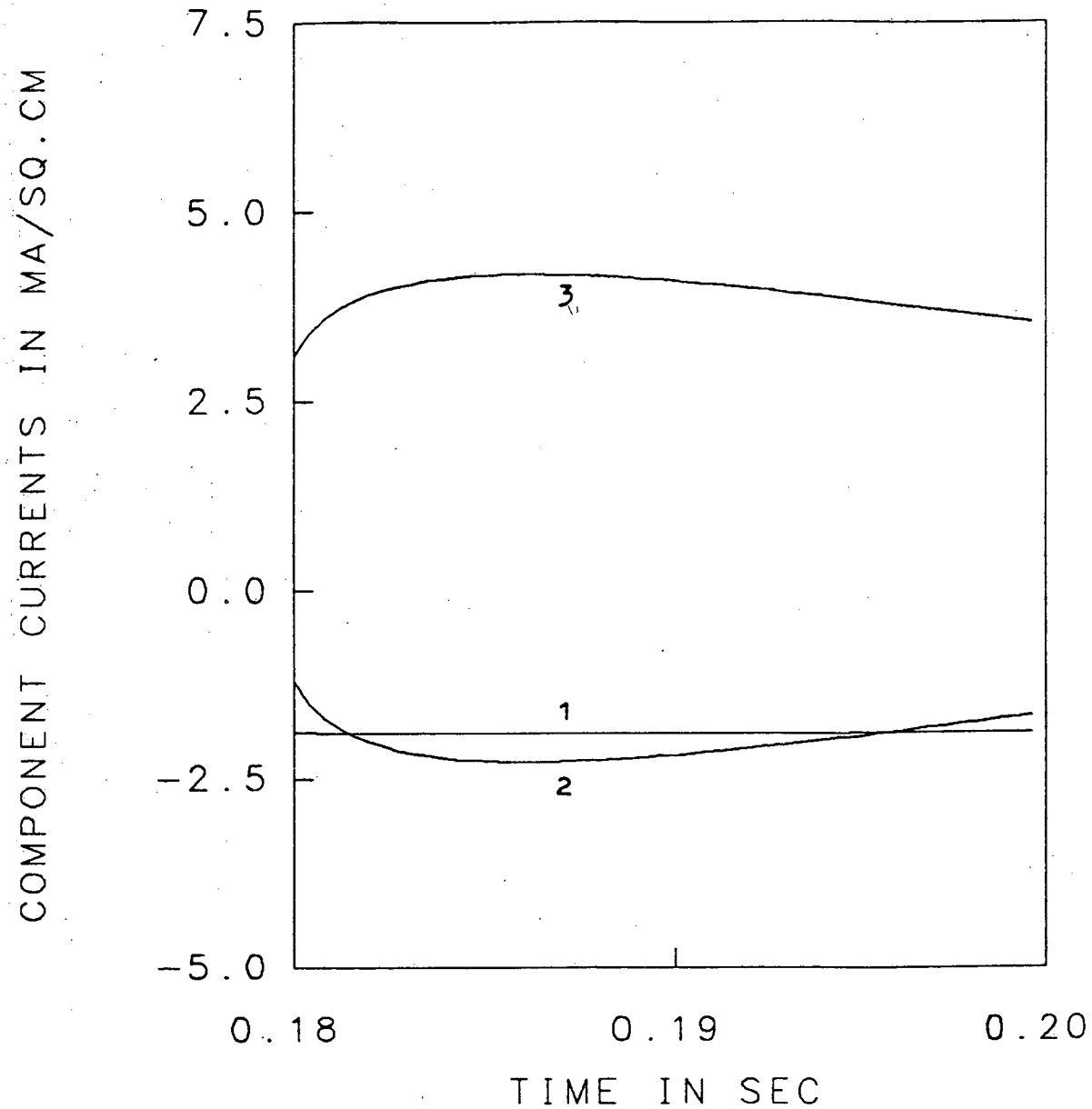
7.5
5.0
2.5
0.0
-2.5
-5.0
COMPONENT CURRENTS IN MA/SQ.CM
3
1
2
0.18
0.19
0.20
TIME IN SEC

Fig. 10

This report was done with support from the Department of Energy. Any conclusions or opinions expressed in this report represent solely those of the author(s) and not necessarily those of The Regents of the University of California, the Lawrence Berkeley Laboratory or the Department of Energy.

Reference to a company or product name does not imply approval or recommendation of the product by the University of California or the U.S. Department of Energy to the exclusion of others that may be suitable.

TECHNICAL INFORMATION DEPARTMENT
LAWRENCE BERKELEY LABORATORY
UNIVERSITY OF CALIFORNIA
BERKELEY, CALIFORNIA 94720